HHS Public Access

Author manuscript

Phys Med Biol. Author manuscript; available in PMC 2019 June 20.

Published in final edited form as:

Phys Med Biol. ; 63(22): 225008. doi:10.1088/1361-6560/aae8b2.

Virtual electrophysiological study as a tool for evaluating efficacy of MRI techniques in predicting adverse arrhythmic events in ischemic patients

Eranga Ukwatta[1,6], **Plamen Nikolov**[3], **Fatemeh Zabihollahy**[2], **Natalia A Trayanova**[3], and **Graham A Wright**[4,5]

[1]School of Engineering, University of Guelph, Guelph, ON, Canada

[2]Department of Systems and Computer Engineering, Carleton University, Ottawa, ON, Canada

[3]Department of Biomedical Engineering, Institute of Computational Medicine, Johns Hopkins University, Baltimore, MD, United States of America

[4]Sunnybrook Research Institute, Sunnybrook Health Science Centre, Toronto, ON, Canada

[5]Department of Medical Biophysics, University of Toronto, Toronto, ON, Canada

Abstract

Myocardial infarct (MI) related indices determined by late gadolinium enhancement (LGE) MRI have been widely investigated in determining patients suitable for implantable cardiovascular-defibrillator (ICD) therapy to complement left ventricular ejection fraction (LV EF). In comparison to LGE-MRI using inversion-recovery fast-gradient-echo (IR-FGRE), T1 mapping techniques, such as multi contrast late enhancement (MCLE), have been shown to provide more quantitative and reproducible estimates of infarct regions. The objective of this study is to use individualized heart computer models in determining the efficacy of IR-FGRE and MCLE techniques in predicting the occurrence of post-MI ventricular tachycardia (VT). Twenty-seven patients with MI underwent LGE-MRI using IR-FGRE and MCLE prior to ICD implantation and were followed up for 6–46 months. Individualized image-based computational models were built separately for each imaging technique; simulations of propensity to VT were conducted with each model. The imaging methods were evaluated by comparing simulated inducibility of VT to clinical outcome (appropriate ICD therapy) in patients. Twelve patients had at least one appropriate ICD therapy for VT at follow-up. For both MCLE and IR-FGRE, the outcomes of the simulations of VT were significantly associated with the events of appropriate ICD therapy. This indicates that, as compared to conventional measurements such as LV EF, the simulations of VT corresponding to both MCLE and IR-FGRE were more sensitive in predicting appropriate ICD therapy in post-MI patients.

[6]Author to whom any correspondence should be addressed. eukwatta@uoguelph.ca.

Disclosure of conflicts of interest

Graham A Wright holds a patent on the MCLE technique, which has been assigned to Sunnybrook Research Institute in Canada.

Keywords

infarct heterogeneity; cardiovascular magnetic resonance; computer simulations of the heart; T1 mapping; late gadolinium enhancement; ischemic heart disease

1. Introduction

Regions of the myocardium may lose viability due to sustained tissue ischemia as a manifestation of coronary artery disease, resulting in myocardial infarction (MI). Infarct regions and surrounding tissue may act as a substrate for post-MI ventricular tachycardia (VT) and fibrillation (VF) (Fishman *et al* 2010), which may eventually lead to sudden cardiac death (SCD). In particular, electrical conduction in the heart through the infarcted regions may lead to anatomically defined re-entry circuits causing VT (Brunckhorst *et al* 2003). For individuals at high risk for SCD, prophylactic insertion of implantable cardioverter defibrillators (ICDs) decreases mortality. Among the non-invasive techniques developed to identify patients with chronic MI at risk for SCD, left ventricular ejection fraction (LV EF), below 35%, remains the primary deciding factor for ICD implantation (Moss *et al* 2002). However, many primary prevention patients with low LV EF may not benefit from ICD implantation, as previous studies have shown that only 20% of the patients out of the study cohort have received ICD shocks for rapid VT and VF at an average annual rate of 7.5% (Bardy *et al* 2005, Fishman *et al* 2010). Thus, recent research has focused on developing alternative non-invasive risk stratification strategies based on the direct measurement of infarct mass or volume (Goldberger *et al* 2014).

Magnetic resonance imaging (MRI) has superior soft tissue contrast and has been established as one of the key modalities to detect abnormalities in the structure and function of the post infarct heart (Wu *et al* 2008, Wu 2017). Previous studies using late gadolinium enhanced cardiac MR (LGE-CMR) imaging using inversion-recovery fast-gradient-echo (IR-FGRE) sequence have demonstrated that both the infarct core (IC) and the surrounding semi-viable tissue, also termed ‘border zone’ (BZ), play an important role in cardiac arrhythmogenesis (Schmidt *et al* 2007, Ismail *et al* 2012). However, the LV blood pool contrast is usually a limiting factor in the conventional LGE-MRI using IR-FGRE technique. While saturation pulses can help, they rely on wash-in of saturated spins, which can yield artifacts in BZs of slow flow adjacent to the myocardium. While employing recently reported gray blood (GB-LGE) techniques may improve myocardial scar identification and localization, most widely used sequences are still conventional black-blood LGE (BB-LGE) and (bright-blood) LGE (Fahmy *et al* 2018). For the BB- and bright-blood LGE techniques, it is especially challenging to distinguish MI from the blood pool, leading to inaccuracies in MI segmentation (Bandettini *et al* 2012). Therefore, quantitative assessment of the infarcts using IR-FGRE requires precise manual or semi-automated segmentation of the myocardium as a pre-processing step. Due to this high dependency on manual myocardial segmentation, the method may also suffer from intra-observer variability (Detsky *et al* 2009, Kellman and Hansen 2014).

Quantitative imaging techniques, such as T1 mapping, measure intrinsic physical properties of the underlying tissue. T1 mapping techniques, as compared to IR-FGRE, have been shown to be more reproducible in determining MI mass (Kellman *et al* 2005, Kellman and Hansen 2014). The T1 mapping techniques enable quantitative assessment of myocardial tissue on a voxel-wise basis, reducing the need for manual segmentation of the myocardial boundaries (Detsky *et al* 2009). Multi-contrast late enhancement (MCLE) is a T1 mapping technique, which enables infarct and cardiac wall assessment in a single acquisition with reduced scan times (Detsky *et al* 2009, Connelly *et al* 2009). In the MCLE technique, the pulse sequence contains an inversion pulse that nulls the signal from the LV blood pool. Due to the nulling of the signal, there is good a contrast between the sub endocardial infarcts and the LV blood pool (Detsky *et al* 2009).

Computational modeling of hearts with MIs has emerged as a promising non-invasive tool to simulate electrical activation of the heart and determine the propensity for re-entrant arrhythmias such as VT (Vadakkumpadan *et al* 2013, Arevalo *et al* 2016, Trayanova *et al* 2017). The computational models are built based on cardiac MR images and can be non-invasively interrogated to yield mechanistic insights into the electrical activity of the heart (Trayanova 2012). Currently, most widely used image-based biomarkers of cardiac structure and function have been limited to global indices, such as LV EF, infarct mass, LV mass, and end-diastolic volume (Yan *et al* 2006). Compared to global indices of cardiac function, computer simulations of VT enable biophysically detailed analysis of electrical activation of the heart. A recent pilot study has shown that these models, as compared to global indices, are more sensitive in predicting ICD therapy (Arevalo *et al* 2016). To accurately represent patient-specific structural changes, these models must incorporate accurate 3D geometric reconstructions of cardiac structure and MI geometry (Ukwatta *et al* 2014, 2015). With the use of computer simulations of VT, there is potential to investigate and compare LGE-MRI using IR-FGRE and MCLE methods in predicting inducibility of VT in post-MI patients. Therefore, the objective of this study was to evaluate individualized computational heart models in determining the efficacy of LGE-MRI using IR-FGRE and MCLE techniques in predicting the occurrence of post-MI VT.

2. Methods

2.1. Study subjects and image acquisition

Our study consists of twenty-seven patients with prior MI eligible for ICD implantation for primary or secondary prevention. The CMR study protocol was approved by the institutional research ethics board at Sunnybrook Research Institute (Toronto, ON, Canada) and all the subjects provided written informed consent. Patients with MR-incompatible implants were excluded from the study. After the CMR examination and ICD implantation, the subjects were followed up in an ICD clinic on a quarterly basis. While there is overlap, four patients in our study are different from the previous study (Yang *et al* 2013).

The CMR studies were conducted using a 1.5 T GE Signa HDx system (GE Healthcare, Milwaukee, USA) with ECG gating and using an eight-channel phased-array cardiac coil. The CMR protocol has been described previously (Detsky *et al* 2009, Yang *et al* 2013). The CMR protocol included LV functional parameter assessment using cine steady state free

precession (SSFP), as well as LGE-CMR using an inversion-recovery fast-gradient-echo (IR-FGRE) and MCLE post double-dose Gd injection. Typical CMR parameters for each method is shown in table 1. For SSFP acquisition, a short-axis oblique 20 phase-resolved images over the whole cardiac cycle were acquired in a breath-hold. Ten to twenty minutes after a double-dose intravenous bolus injection of Gd-DTPA (Magnevist®, Bayer Inc., Canada; Equivalent to 0.2 mmol kg^{-1}), LGE-CMR images using IR-FGRE were acquired followed by MCLE images, using the same short-axis oblique localization as the cine SSFP images. Depending on the null point of normal myocardium, the inversion time (TI) varied from 200 to 300 ms in IR-FGRE. Approximately 20 heartbeats (18 s breath-holds on average) were required to produce a single LGE-CMR image using IR-FGRE. For MCLE, a segmented SSFP readout was used following an inversion-recovery pulse, providing 20 cardiac phase-resolved images at different TIs. The MCLE pulse sequence required approximately 13 heartbeats to acquire. The first heartbeat established a steady state and the 12 following heartbeats enabled acquisition of 20 separate images during different phases of the cardiac cycle at different effective TIs. Data acquisition was continuously implemented in a segmented fashion between each TI. The MCLE sequence implemented a delay time of 500 ms and total sequence acquisition required a breath-hold of about 11 s.

According to clinical guidelines, all the patients received a single or dual ICD implantation. All patients were followed in an ICD clinic at intervals of three months and more frequently (if device shocks were delivered) for 6–46 months with a median follow-up of 30 months. Two experienced electrophysiologists reviewed the ICD data for the relevant ventricular arrhythmic events. The primary outcome measure was appropriate ICD therapy, which was defined as a shock for VT, VF, or any ventricular arrhythmic event identified as sustained VT or VF (Yang *et al* 2013). In this study, appropriate ICD therapy refers to an ICD event which was triggered for a single rhythm episode regardless of the total number of actual shocks that were needed for termination of tachycardia (Yang *et al* 2013).

2.2. Image processing of MRI data

Cine SSFP images were analyzed using CMR (Steinbeck *et al* 2009) software (Circle Cardiovascular Imaging, Calgary, Canada), where LV functional parameters of LV EF, LV volumes at end-systolic (LV ESV) and enddiastolic phase (LV EDV), stroke volumes (SV) and LV mass at end-diastolic phase were measured.

In IR-FGRE and MCLE images, the epi- and endo-cardial boundaries of the LV and RV were manually contoured in the image slices by an expert using the ImageJ software program (National Institutes of Health, Bethesda, MD, USA) as shown in figure 1. From the 20 phases of the MCLE images, a diastolic phase after signal recovery was chosen for myocardial segmentation. Due to the inherent differences of IR-FGRE and MCLE, two different approaches were used for infarct segmentation.

For the IR-FGRE images, the infarct was segmented as IC and BZ using the full-width at half maximum (FWHM) method (Schmidt *et al* 2007), for which the pre-segmented LV myocardium was used as the initial region. The expert chooses a region of interest in the remote healthy myocardium and the peak intensity in the infarct. The IC was considered as the regions with intensities above the half of the peak intensity of the infarct. The BZ was

computed as the regions with intensity above peak of the remote region but below the half of the peak intensity of the infarct. Figure 1(b) shows segmentations of the IC and BZ regions for an example IR-FGRE image.

The MCLE images were first pre-processed one slice at a time to create the T_1^* and steady state maps (Detsky *et al* 2009). From the 20 phases across the cardiac cycle, more than three phases at the diastolic window with minimal cardiac motion were chosen for exponential curve fitting. Having more phases with minimal cardiac motion will lead to superior T_1^* maps. Figure 2(a) shows a basal slice of an example MCLE image and ten phases with minimal cardiac motion chosen out of 20 phases. Data fitting of signal intensities acquired at multiple inversion times is then used to create the T_1^* and the steady state maps as shown in figures 2(b) and (c). The infarcts were segmented as IC and BZ using a clustering approach based on fuzzy c-means, using both T_1^* and steady state maps (Detsky *et al* 2009). Unlike the infarct segmentation approach for IR-FGRE, the precise segmentation of the myocardial boundaries is not required for MCLE. The algorithm considers four clusters representing the IC, BZ, blood pool and healthy myocardium. This algorithm determines the probability of each voxel belonging to each of the clusters based on a distance metric in a scatter plot of T_1^* and steady state values. The IC and healthy myocardium regions were classified as voxels with probabilities greater than 75% of belonging to the clusters of the IC and health myocardium, respectively (Detsky *et al* 2009). The BZ region was defined as voxels with a probability smaller than 75% of belonging to either IC or healthy myocardium and a probability of greater than 25% belonging to the other cluster (Detsky *et al* 2009). Figure 2(d) shows segmentation results of the IC and BZ regions using the fuzzy c-means clustering approach for the T_1^* and steady state maps.

Using the segmented geometry of myocardium and infarcts, finite element models (FEM) were built separately for both IR-FGRE and MCLE images. To create a three-dimensional (3D) model, ventricular geometry was reconstructed from the myocardial boundaries at an isotropic resolution of 0.4 mm using an interpolation method based on variational implicit functions (Ukwatta *et al* 2016). Finally, the 3D geometry of the infarct was reconstructed from the infarct segmentations using an interpolation technique we developed based on LogOdds (Ukwatta *et al* 2015). The 3D geometry of the total infarct region and IC was first reconstructed using the LogOdds method. The reconstruction for the BZ was then obtained as the relative complement of the IC, where infarct reconstruction was considered as the union. All image processing tasks were performed in the Matlab computing environment (Mathworks Inc., Natick, MA, USA) installed on a personal computer equipped with a 2.3 GHz Intel Core i7 CPU, 12 GB of RAM and the Windows operating system.

2.3. Simulation of cardiac electrophysiology

The pipeline for generating models from IR-FGRE images has been described previously (Arevalo *et al* 2016, Trayanova *et al* 2017, 2018). Using the ventricular reconstruction, and the infarct reconstructions, two FEMs, one incorporating infarct geometries reconstructed from IR-FGRE, and the other with infarct zone geometries built from the MCLE, were created. Figure 3 shows two FEMs created from IR-FGRE and MCLE images of a patient

heart, where the geometries of the IC and BZ appears different. The fiber orientations for the models were estimated using a rule-based method (Bayer *et al* 2012).

We conducted simulations of VT similar to the previous approaches (Arevalo *et al* 2016, Trayanova *et al* 2017, 2018). Electrical propagation was modeled using the monodomain formulation (Plank *et al* 2008). Intracellular conductivities in the normal myocardium were assigned such that the resulting conduction velocity matched those recorded in human ventricular experiments (Moreno *et al* 2011). To represent connexin 43 remodeling and lateralization in the remodeled BZ, transverse conductivity was decreased by 90%, resulting in increased tissue anisotropy (Yao *et al* 2003). The IC was modeled as passive tissue with zero conductivity.

The Ten Tusscher human ventricular action potential model was used to represent the membrane kin etics in the healthy myocardium (ten Tusscher *et al* 2004). For the remodeled BZ, the action potential model was modified to represent electrophysiological changes that have been observed experimentally (reduction in peak sodium current to 38% of the normal value (Pu and Boyden 1997), in peak L-type calcium current to 31% of normal (Dun *et al* 2004), and in peak potassium currents IKr and IKs to 30% and 20% of the maximum (Jiang *et al* 2000), respectively) (Arevalo *et al* 2016). These modifications resulted in BZ action potential morphology that had decreased upstroke velocity, decreased amplitude, and increased duration, consistent with experimental recordings (Decker and Rudy 2010).

Simulations of VT induction were also performed in all models by applying at the apex and RV insertion point a programmed electrical stimulation (PES) protocol similar to the one used in the clinic (Wellens *et al* 1985). The PES protocol consisted of six pacing (S1) stimuli with a coupling interval of 350 ms, followed by a premature stimulus (S2) whose cycle length was shortened until sustained VT was initiated or the last stimulus failed to capture. If needed, two additional extra-stimuli were delivered to attempt arrhythmia induction. An arrhythmia was classified as sustained if it persisted for at least two seconds (Arevalo *et al* 2016). All simulations were performed using the open-source software package CARPentry on a parallel computing platform (Rodrguez *et al* 2005, Bishop *et al* 2007, Rantner *et al* 2012, Arevalo *et al* 2016, CARPentry Developers 2017).

A true positive (TP) is considered as simulated sustained VT matching the appropriate ICD therapy (i.e. shocks for VT or VF) at follow-up. A true negative (TN) is considered as non-inducibility of the simulated heart model matching no delivered shocks to the patient. An event is denoted a false positive (FP) when the simulation incorrectly predicts appropriate ICD therapy. An event is considered a false negative (FN) when the simulation fails to predict an appropriate ICD therapy. For both MI MRI imaging technique, we computed sensitivity (TP/(TP+FN)), specificity (TN/(TN+FP)), positive predictive value (TP/(TP+FP)) and negative predictive value (TN/(TN+FN)) of the simulations of VT.

For the patient characteristics and imaging indices, we expressed continuous variables as mean ± SD and categorical data as numbers (percentages). For statistical analysis, we used and the Student's *t*-test for continuous variables and Fisher exact test for categorical data. We also conducted multiple logistic regression to evaluate the prediction of appropriate ICD

therapy in patients based on two types of measurements: one involving the NYHA functional class, LV EF, LV EDV, and LV ESV and the other involving IC and BZ masses. All statistical analyses were performed using IBM SPSS Statistical version 19 (IBM Corporation 2010), in which results were considered significant when the probability of making a type I error was less than 5% ($p < 0.05$).

3. Results

Table 2 shows a summary of patient data set characteristics including CMR-derived LV functional information. For each characteristic, the statistical significance was tested for the patients with and without ICD therapy. None of the indices were significantly different between the patients with and without ICD therapy similar to previous observations (Yang *et al* 2013).

Table 3 lists CMR MI heterogeneity measurements for patient groups with and without ICD therapy. The MIs were normalized to LV mass. Similar to the results of the previous study by Yang *et al* (2013), The BZ mass determined by MCLE was significantly different between the groups with and without ICD therapy. None of the other infarct masses determined by both the MRI techniques was significantly different between the patients with and without ICD therapy, although such quantities were typically larger in patients undergoing appropriate ICD therapy.

We performed multiple logistic regression where NYHA functional class, LV EF, LV ESV and LV EDV were considered as independent variables. The model failed to show a statistically significant difference ($p = 0.375$) between the patients with and without appreciate ICD therapy. The model yielded a sensitivity, specificity, positive predictive value, and negative predictive value of 66.7%, 61.5%, 61.5%, and 66.7, respectively. In the receiver operating characteristic (ROC) analysis, the area under the curve (AUC) was 0.67 with 95% confidence intervals of 0.54–0.83.

Figure 3 shows activation maps of a single beat of VT for models, corresponding to both MCLE and IR-FGRE images, with re-entry circuit activity shown with white arrows near infarct location. The activation maps in simulations were derived by determining, at each node of the finite element meshes, the instant in time at which the upstroke of the action potential at that node reached a threshold of 0 mV. Due to errors that occurred in creating the FEM of the heart using the scanIP software (Synopsys, Mountain View, CA, USA), two patients out of 27 were excluded from further analysis.

Summary of results for computer simulations of VT for models built with LGE-MRI using IR-FGRE and MCLE are shown in table 4. The p-values corresponding to heart models built using both MCLE and IR-FGRE indicate that there is a significant association between simulated VT inducibility and the appropriate ICD therapy. For heart models built using MCLE, the odds ratio indicates that the patients with simulated VT inducibility have about 27.5 times greater odds of having appropriate ICP therapy than the patients with no VT inducibility. The simulations using MCLE images yielded a higher sensitivity and specificity, as compared to the ones using IR-FGRE images.

We also evaluated the predictability of appropriate ICD therapy of BZ mass using cut-off thresholds from 10% to 17% as shown in table 5. Sensitivity and specificity of predicting appropriate ICD therapy from BZ volume at these various thresholds for both MRI techniques were smaller than that of using the simulations of VT. We also performed multiple logistic regression where IC and BZ masses were considered as independent variables. For IC and BZ masses determined by MCLE, the model obtained a sensitivity, specificity, positive predictive value, and negative predictive value of 69.2%, 66.7%, 69.2% and 66.7%, respectively. In the ROC analysis, the AUC was 0.73 with 95% confidence intervals of 0.49 to 0.87. For IC and BZ masses determined by IR-FGRE, the model reported a sensitivity, specificity, positive predictive value and negative predictive value of 83.3%, 61.5%, 66.7% and 80.0%, respectively. In the ROC analysis, the AUC was 0.71 with 95% confidence intervals of 0.50–0.87.

4. Discussion and conclusion

For individuals at high risk for SCD, ICD implantation is a life-saving intervention, terminating VF and/or VT and restoring normal rhythm (Steinbeck *et al* 2009). The LV EF < 35% metric is the key deciding factor for ICD implantation in primary prevention patients. Average annual ICD firing rates of primary prevention patients are around 7.5%, where about 20% of the patients received shocks (Bardy *et al* 2005). Recent studies have shown that patients with LV EF > 35% may also benefit from ICD implantation (Deng *et al* 2016). Therefore, there is a need to develop novel risk stratification strategies to identify patients at risk of SCD (Fishman *et al* 2010). In particular, studies have shown that infarct mass relative to LVM determined by LGE-MRI techniques as a sensitive measurement in predicting appropriate ICD therapy (Boyé *et al* 2011). However, predicting the ICD therapy in a given individual will require defining cut-off thresholds for infarct mass, which highly depend on the segmentation method and may not be sensitive or specific enough in predicting therapy on a personalized basis. Therefore the objective of this study was to evaluate individualized heart computer models in determining the efficacy of IR-FGRE and MCLE techniques in predicting the occurrence of post-MIVT.

Due to the advancement of computational modeling along with the development of whole heart MRI acquisition, virtual models of the patient hearts can be created for a detailed assessment of cardiac electrophysiology in the heart (Arevalo *et al* 2016, Trayanova *et al* 2017). In this preliminary study, we demonstrated that computer simulations of VT in patient-specific models could be used in stratifying patient risk for SCD using computer simulations of VT inducibility. Simulations of VT inducibility interrogate the detailed electrical activation of the heart in the MI-remodeled cardiac substrate, which is directly dependent on the reconstruction of infarct and ventricular geometry (Prakosa *et al* 2014, Ukwatta *et al* 2015, 2016).

We compared measurements determined by MCLE and IR-FGRE to demonstrate any potential differences in the two techniques should the clinicians decide to choose one of the methods as an alternative to the other in the diagnosis and prognosis of post-MI patients. In this study, we observed that our results on patient characteristics and infarct masses were comparable to the ones reported by Yang *et al* (2013). Except for the BZ mass determined by

the MCLE technique, none of the other indices was statistically significant between the patients with and without appropriate ICD therapy. The differences in MI masses determined by MCLE and IR-FGRE may arise due to several factors: difference in information content in the T_1^* map and steady state data in MCLE versus just signal intensity in IR-FGRE, different ways of processing a two distinct features spaces (two parameter fit versus a single value); choice of image segmentation methods; signal intensity in IR-FGRE is a nonlinear function of $T1$ and can be confounded by undesirable factors such as coil shading; and differences in image resolution. Even when the same image processing method (e.g. FWHM) was used to segment both T1 mappings, we experimentally observed differences in the estimation of BZ and IC masses.

One of the main errors in infarct quantification in IR-FGRE stems from the manual segmentation of the LV endocardium. The MCLE technique uses SSFP readout immediately after an inversion pulse, which permits visualization of infarction as an area of fast $T1$ recovery with the simultaneous nulling of blood pool and viable myocardium. A $T1$ mapping technique, such as MCLE, does not require precise myocardial segmentation and hence may avoid such potential errors in infarct quantification.

For both MCLE and IR-FGRE, the outcome of simulations of VT (i.e. simulated VT inducibility) was significantly different between the patients with and without ICD therapy. Simulations of VT inducibility, as compared to cut-off thresholds defined on peri-infarct BZ mass, had a better operating point for sensitivity and specificity irrespective of the MRI technique used to quantify the infarct. This suggests that, as compared to patient characteristics and infarct masses, the simulations of VT were more sensitive in predicting appropriate ICD therapy in post-MI patients.

Furthermore, the simulations of VT inducibility using MCLE images yielded higher sensitivity (83.3% versus 66.7%) and specificity (84.6% versus 76.9%) in predicting appropriate ICD therapy compared to those using IR-FGRE images. While this trend is inconclusive due to the limited number of data points in our study cohort, it is in agreement with the higher predictive capability of mass-based measurement determined by MCLE technique (Yang *et al* 2013), which may be partially due to the larger BZ mass determined by the MCLE technique. Arevalo *et al* (2013), using computer simulations of VT, have shown that larger BZs in models lead to increased inducibility of VT.

This study has several limitations. Our study was retrospective and included only a small patient cohort due to resource constraints. Although we observed significant differences in some indices, such as BZ mass determined by MCLE, statistical analysis could have been more robust with a larger number of patients. Due to the limited number of data points in our study cohort, the sensitivity and specificity values are sensitive to single data points. Therefore, the results should be interpreted as hypothesis generating. Although we observed virtual models built using MCLE yielded higher values for sensitivity and specificity, it is not possible to determine which MRI technique is more accurate in quantifying infarct structure, without digital histopathology data of the hearts. One clear indication is that irrespective of the imaging method, the addition of simulations of VT using MRI-determined MI maps has great potential for improving specificity.

Our image processing pipeline consists of several manual segmentation steps. From those steps, the most time consuming one was the segmentation of the LV and RV, which was subject to high observer variability. Automated image analysis methods may have alleviated the measurement burden while potentially increasing the reproducibility of the segmentations.

A previous study (Ukwatta *et al* 2016) has shown the effect of the choice of image segmentation method on the outcomes of simulations of VT simulations. Therefore, the choice of image segmentation methods may have influenced the outcomes of VT simulations in our study. While it is interesting to investigate the effect of choosing different levels of intensity thresholds on the outcomes of simulations, it will be very time consuming thus is prohibitive in practice. Currently, a simulation of VT for a single heart model takes about six hours of computational time on a parallel computing platform. This also prevents us from optimizing the parameters of the pipeline.

The reported sensitivity and specificity depend on VT simulations on the number of points used to virtually stimulate the heart, where previous studies have used up to 18 pacing points (Arevalo *et al* 2016). There is a potential for individualized heart models to further improve the sensitivity and specificity by investigating the optimal operating point while the number of virtually stimulated points are varied.

Acknowledgment

E Ukwatta acknowledges funding support from Natural Sciences and Engineering Research Council of Canada (NSERC) Discovery grant and Johns Hopkins Biomedical Engineering Centennial Postdoctoral Fellowship. This study was supported by Canadian Institutes of Health Research (CIHR) grant (MOP93531 to GAW) and the National Institute of Health (NIH) Director's Pioneer Award (DP1HL123271 to NAT).

References

Arevalo HJ. et al. 2016; Arrhythmia risk stratification of patients after myocardial infarction using personalized heart models. Nat. Commun. 7:11437. [PubMed: 27164184]

Arevalo H, Plank G, Helm P, Halperin H and Trayanova N 2013 Tachycardia in post-infarction hearts: insights from 3D image-based ventricular models PLoS One 8 e68872 [PubMed: 23844245]

Bandettini WP. et al. 2012; Multicontrast delayed enhancement (MCODE) improves detection of subendocardial myocardial infarction by late gadolinium enhancement cardiovascular magnetic resonance: a clinical validation study. J. Cardiovasc. Magn. Reson. 14:83. [PubMed: 23199362]

Bardy GH et al. 2005 Amiodarone or an implantable cardioverter–defibrillator for congestive heart failure New Engl. J. Med 352 225–37

Bayer JD, Blake RC, Plank G and Trayanova NA 2012 A novel rule-based algorithm for assigning myocardial fiber orientation to computational heart models Ann. Biomed. Eng 40 2243–54 [PubMed: 22648575]

Bishop M, Rodriguez B, Qu F, Efimov IR, Gavaghan D and Trayanova N 2007 The role of photon scattering in optical signal distortion during arrhythmia and defibrillation Biophys. J 93 3714–26 [PubMed: 17978166]

Boyé P et al. 2011 Prediction of life-threatening arrhythmic events in patients with chronic myocardial infarction by contrast-enhanced CMR JACC Cardiovasc. Imaging 4 871–9 [PubMed: 21835379]

Brunckhorst CB, Stevenson WG, Soejima K, Maisel WH, Delacretaz E, Friedman PL and Ben-Haim SA 2003 Relationship of slow conduction detected by pace-mapping to ventricular tachycardia re-entry circuit sites after infarction J. Am. Coll. Cardiol 41 802–9 [PubMed: 12628726]

CARPentry Developers 2017 CARPentry Modeling Environment Documentation (https://carpentry.medunigraz.at/carputils/#) (Accessed 23 August 2018)

Connelly KA et al. 2009 Multicontrast late gadolinium enhancement imaging enables viability and wall motion assessment in a single acquisition with reduced scan times J. Magn. Reson. Imaging 30 771–7 [PubMed: 19787723]

Decker KF and Rudy Y 2010 Ionic mechanisms of electrophysiological heterogeneity and conduction block in the infarct border zone Am. J. Physiol. Circ. Physiol 299 H1588–97

Deng D, Arevalo HJ, Prakosa A, Callans DJ and Trayanova NA 2016 A feasibility study of arrhythmia risk prediction in patients with myocardial infarction and preserved ejection fraction Europace 18 iv60–6 [PubMed: 28011832]

Detsky JS, Paul G, Dick AJ and Wright GA 2009 Reproducible classification of infarct heterogeneity using fuzzy clustering on multicontrast delayed enhancement magnetic resonance images IEEE Trans. Med. Imaging 28 1606–14 [PubMed: 19783498]

Dun W, Baba S, Yagi T and Boyden PA 2004 Dynamic remodeling of K + and Ca2 + currents in cells that survived in the epicardial border zone of canine healed infarcted heart Am. Physiol. Soc 287 H1046–H1054

Fahmy AS. et al. 2018; Gray blood late gadolinium enhancement cardiovascular magnetic resonance for improved detection of myocardial scar. J. Cardiovasc. Magn. Reson. 20:22. [PubMed: 29562921]

Fishman GI et al. 2010 Sudden cardiac death prediction and prevention: report from a National Heart, Lung, and Blood Institute and Heart Rhythm Society workshop Circulation 122 2335–48 [PubMed: 21147730]

Goldberger J, Basu A, Boineau R and Buxton A 2014 Risk stratification for sudden cardiac death Circulation 129 516–26 [PubMed: 24470473]

Ismail TF, Prasad SK and Pennell DJ 2012 Prognostic importance of late gadolinium enhancement cardiovascular magnetic resonance in cardiomyopathy Heart 98 438–42 [PubMed: 22128204]

Jiang M, Cabo C, Yao JA, Boyden PA and Tseng GN 2000 Delayed rectifier K currents have reduced amplitudes and altered kinetics in myocytes from infarcted canine ventricle Cardiovascular Res. 48 34–43

Kellman P and Hansen MS 2014 T1-mapping in the heart: accuracy and precision J. Cardiovasc. Magn. Reson 16 1–20 [PubMed: 24387349]

Kellman P, Chung Y-C, Simonetti OP, McVeigh ER and Arai AE 2005 Multicontrast delayed enhancement provides improved contrast between myocardial infarction and blood pool J. Magn. Reson. Imaging 22 605–13 [PubMed: 16215969]

Moreno JD. et al. 2011; A computational model to predict the effects of class I anti-arrhythmic drugs on ventricular rhythms. Sci. Transl. Med. 3:98ra83.

Moss A, Zareba W, Hall W and Klein H 2002 Prophylactic implantation of a defibrillator in patients with myocardial infarction and reduced ejection fraction New Engl. J. Med 346 877–83 [PubMed: 11907286]

Plank G et al. 2008 From mitochondrial ion channels to arrhythmias in the heart: computational techniques to bridge the spatio-temporal scales Phil. Trans. R. Soc. A 366 3381–409 [PubMed: 18603526]

Prakosa A et al. 2014 Methodology for image-based reconstruction of ventricular geometry for patient-specific modeling of cardiac electrophysiology Prog. Biophys. Mol. Biol 115 226–34 [PubMed: 25148771]

Pu J and Boyden PA 1997 Alterations of Na+ currents in myocytes from epicardial border zone of the infarcted heart: a possible ionic mechanism for reduced excitability and postrepolarization refractoriness Am. Heart Assoc 81 110–9

Rantner L, Arevalo H, Constantino J, Efimov I, Plank G and Trayanova N 2012 Three-dimensional mechanisms of increased vulnerability to electric shocks in myocardial infarction: altered virtual electrode polarizations and conduction delay in the peri-infarct zone J. Physiol 590 4537–51 [PubMed: 22586222]

Rodrguez B, Li L, Eason J, Efimov I and Trayanova N 2005 Differences between left and right ventricular chamber geometry affect cardiac vulnerability to electric shocks Circ. Res 97 168175

Schmidt A et al. 2007 Infarct tissue heterogeneity by magnetic resonance imaging identifies enhanced cardiac arrhythmia susceptibility in patients with left ventricular dysfunction Circulation 115 2006–14 [PubMed: 17389270]

Steinbeck G et al. 2009 Defibrillator implantation early after myocardial infarction New Engl. J. Med 361 1427–36 [PubMed: 19812399]

ten Tusscher KHWJ, Noble D, Noble PJ and Panfilov AV 2004 A model for human ventricular tissue Am. J. Physiol. Circ. Physiol 286 H1573–89

Trayanova NA 2012 Computational cardiology: the heart of the matter ISRN Cardiol. 2012 1–15

Trayanova NA, Boyle PM and Nikolov PP 2018 Personalized imaging and modeling strategies for arrhythmia prevention and therapy Curr. Opin. Biomed. Eng 5 21–8 [PubMed: 29546250]

Trayanova NA, Pashakhanloo F, Wu KC and Halperin HR 2017 Imaging-based simulations for predicting sudden death and guiding ventricular tachycardia ablation Circ. Arrhythmia Electrophysiol 10 e004743

Ukwatta E et al. 2015 Image-based reconstruction of three-dimensional myocardial infarct geometry for patient-specific modeling of cardiac electrophysiology Med. Phys 42 4579–90 [PubMed: 26233186]

Ukwatta E et al. 2016 Myocardial infarct segmentation from magnetic resonance images for personalized modeling of cardiac electrophysiology IEEE Trans. Med. Imaging 35 1408–19 [PubMed: 26731693]

Ukwatta E, Yuan J, Qiu W, Wu KC, Trayanova N and Vadakkumpadan F 2014 Myocardial infarct segmentation and reconstruction from 2D late-gadolinium enhanced magnetic resonance images Med. Image Comput. Comput. Assist. Interv 17 554–61 [PubMed: 25485423]

Vadakkumpadan F, Arevalo H, Jebb A, Wu KC and Trayanova N 2013 Image-based patient-specific simulations of ventricular electrophysiology for sudden arrhythmic death risk stratification Circulation 128 A18014

Wellens HJJ, Brugada P and Stevenson WG 1985 Programmed electrical stimulation of the heart in patients with life-threatening ventricular arrhythmias: what is the significance of induced arrhythmias and what is the correct stimulaton protocol? Circulation 72 1–7 [PubMed: 4006120]

Wu KC. 2017; Sudden cardiac death substrate imaged by magnetic resonance imaging: from investigational tool to clinical applications. Circ. Cardiovasc. Imaging. 10:e005461. [PubMed: 28637807]

Wu KC et al. 2008 Late gadolinium enhancement by cardiovascular magnetic resonance heralds an adverse prognosis in nonischemic cardiomyopathy J. Am. Coll. Cardiol 51 2414–21 [PubMed: 18565399]

Yan AT et al. 2006 Characterization of the peri-infarct zone by contrast-enhanced cardiac magnetic resonance imaging is a powerful predictor of post-myocardial infarction mortality Circulation 114 32–9 [PubMed: 16801462]

Yang Y. et al. 2013; Multi-contrast late enhancement CMR determined gray zone and papillary muscle involvement predict appropriate ICD therapy in patients with ischemic heart disease. J. Cardiovasc. Magn. Reson. 15:57. [PubMed: 23803259]

Yao J-A, Hussain W, Patel P, Peters NS, Boyden PA and Wit AL 2003 Remodeling of gap junctional channel function in epicardial border zone of healing canine infarcts Circ. Res 92 437–43 [PubMed: 12600896]

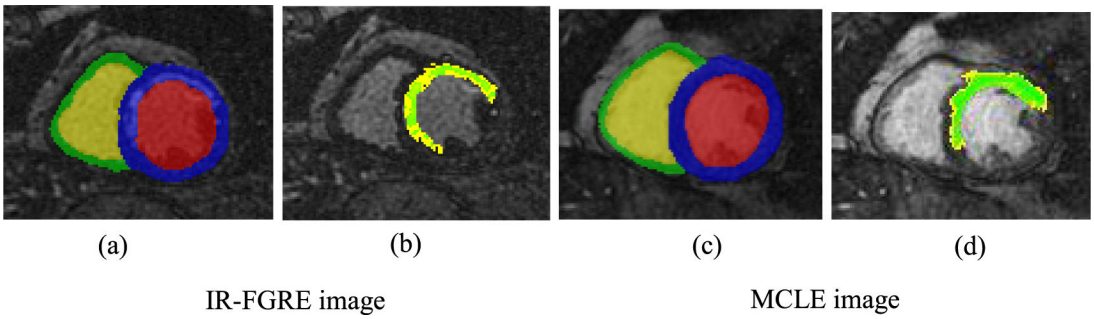

Figure 1.

IR-FGRE and MCLE images were segmented using semi-automated image analysis methodologies to build patient-specific models of the heart. All parts (a)–(d) are the same slice and phase of a cardiac cycle. For the IR-FGRE images, the infarct was segmented using the FWHM technique from pre-segmented myocardium. (a) Manually segmented myocardium of the LV and RV shown in color blue and green, respectively. (b) The IC and BZ are shown in green and yellow, respectively. For the MCLE images, the infarct was segmented using the fuzzy c-means clustering approach. (c) segmented myocardium of the LV and RV shown in color blue and green, respectively. (d) The IC and BZ are shown in green and yellow, respectively.

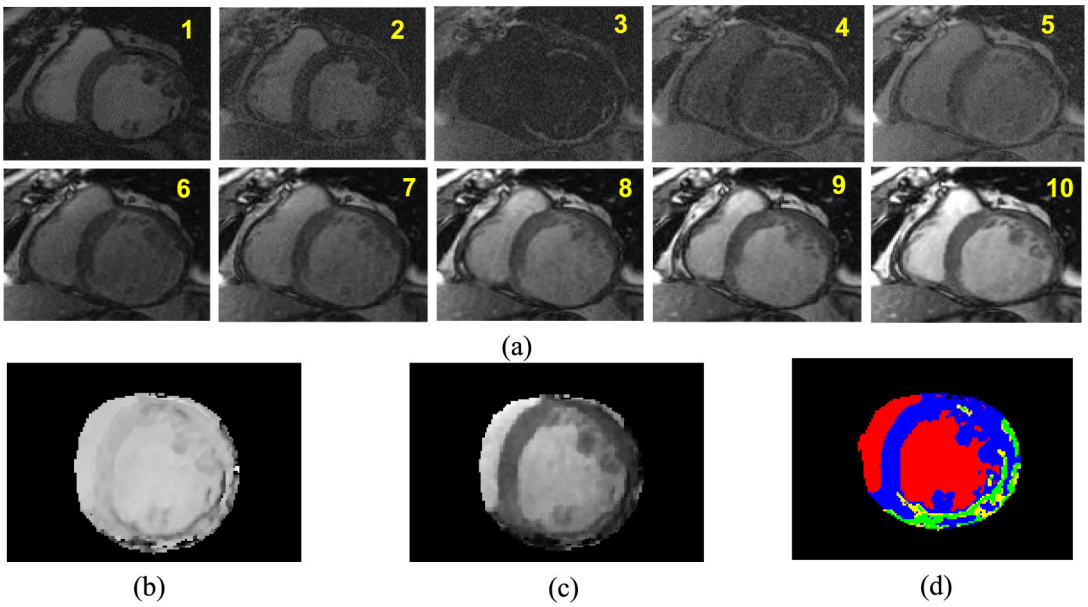

Figure 2.

(a) Basal slice of an example MCLE image and ten different phases with minimal cardiac motion chosen out of 20 phases; (b) T_1^* map and (c) steady state map that were generated using the exponential curve fitting approach for the image slice in (a); and (d) segmentation of the infarct is performed using a fuzzy c-means clustering approach, which utilizes T_1^* map and steady state map for classification. The segmented IC and BZ regions are shown in green and yellow, whereas the healthy myocardium and blood pool are shown in blue and red.

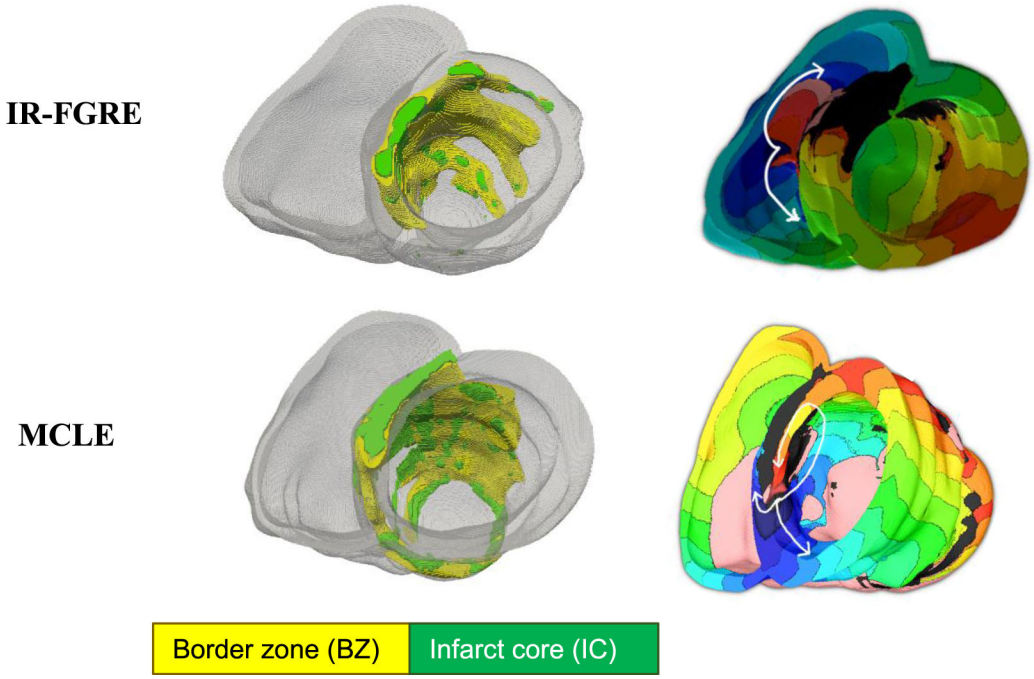

Figure 3.

(Left) FEM models, created using IR-FGRE and MCLE images, depicting IC and BZ locations in green and yellow, respectively. (Right) Corresponding activation maps of a single beat of VT for a model with re-entry circuit activity shown with white arrows near infarct location.

Table 1.

CMR imaging parameters for three types of MRI acquisitions used in this work.

	SSFP	IR-FGRE	MCLE
Bandwidth (rBW)	±125 kHz	±31.5 kHz	±125 kHz
Flip angle	45°	20°	30°
Views per segment (VPS)	16	20	16
TR/TE (ms)	3.7/1.6	6.0/3.0	3.3/1.4
Field of view (FOV) (cm)	32	32	32
Image matrix	256 × 192	192 × 192	192 × 192
In-plane resolution (mm^2)	1.5 × 1.5	1.5 × 1.5	1.37 × 1.37
Slice thickness (mm)	8	8	8
Number of slicers per acquisition	8–10	8–10	8–10
Total data acquisition time per slice	10–20 s breath-hold	10–20 s breath-hold	11 s breath-hold
Number of excitations (NEX)	1	2	1

Table 2.

Patient characteristics of the 27 study subjects. For each characteristic, the statistical significance was tested for the patients with and without ICD therapy. None of the indices was significantly different between the patients with and without ICD therapy.

Patient characteristics	**Total (*n* = 27)**	**With ICD therapy (*N* = 12)**	**Without ICD therapy (*N* = 15)**	***P* value**
Age, years old	62.3 ± 11.2	63.7 ± 9.3	61.2 ± 12.8	0.58
Male	24 (89%)	10 (83.3%)	13 (86.7%)	0.8
Primary prevention	16 (59%)	6 (50%)	10 (66.7%)	0.49
NYHA functional class	1.44 ± 0.97	1.8 ± 1.0	1.2 ±0.9	0.15
Anti-arrhythmic	5(18%)	2(16.7%)	3 (20.0%)	0.83
Smoking	15 (56%)	6 (50%)	8 (61.5%)	0.62
Hypertension	20 (74%)	10 (83%)	9 (60%)	0.34
Diabetes	5 (18%)	2 (16.7%)	3 (20.0%)	0.83
Hyperlipidemia	22 (81%)	11 (91.7%)	11 (73.3%)	0.24
QRS duration (ms)	113.7 ± 28.6	120.7 ± 36.4	108.1 ± 20.1	0.27
Left bundle-branch block	5(18%)	3 (27.3%)	2(13.3%)	0.51
CMR LV function				
LV EF (%)	25.7 ± 8.65	22.1 ± 8.5	28.6 ± 9.2	0.053
LV ESV (ml)	174.9 ± 79.8	203.5 ± 82.7	157.6 ± 76.2	0.11
LV EDV (ml)	231.8 ± 81.1	256.2 ± 82.2	212.2 ± 77.4	0.17
LV SV (ml)	56.5 ± 18.2	52.7 ± 18.9	59.6 ± 17.6	0.34
LVM (g)	106.6 ± 32.2	110.9 ± 34.8	103.2 ± 30.8	0.55

Table 3.

Infarct masses estimated using the MCLE and IR-FGRE techniques, reported separately for the 27 study subjects with and without ICD therapy. The reported masses were normalized by the left ventricular mass (LVM). From all the reported indices, only the BZ mass determined by MCLE was significantly different between the groups with and without ICD therapy.

	With ICD therapy (*n*= 12)		**Without ICD therapy (*n* = 15)**		***P* value**	
	MCLE	**IR-FGRE**	**MCLE**	**IR-FGRE**	**MCLE**	**IR-FGRE**
BZ/LVM (%)	17.4 ± 6.5	11.1 ± 6.3	12.0 ± 5.6	9.8 ± 5.3	0.044	0.58
Core MI/LVM (%)	29.8 ± 8.6	22.7 ± 14.9	23.1 ± 12.9	19.5 ± 11.7	0.094	0.60
Total MI/LVM (%)	47.2 ± 13.1	33.8 ± 20.7	35.1 ± 18.3	29.7 ± 17.3	0.081	0.54

Table 4.

Summary of results for computer simulations of VT for predicting appropriate ICD therapy using models built using LGE-MRI using IR-FGRE and MCLE for 25 study subjects. Due to errors that occurred in creating the heart models, two patients out of 27 were excluded from this analysis. For both MCLE and IR-FGRE, Fisher exact test results showed that the simulated VT inducibility was significantly associated with the events of appropriate ICD therapy.

	MCLE	IR-FGRE
Number of patients	25	25
TP	10 (40%)	8 (32%)
TN	11 (44%)	10 (40%)
FP	2 (8%)	3 (12%)
FN	2 (8%)	4 (16%)
p value	0.0012	0.0472
Odds ratio	27.5	6.67
Confidence interval of the odds ratio	[3.24 233.47]	[1.14 38.83]
Sensitivity (%)	83.3	66.7
Specificity (%)	84.6	76.9
Positive predictive value (%)	83.3	72.7
Negative predictive value (%)	84.6	71.4

Table 5.

Sensitivity and specificity of predicting appropriate ICD therapy using peri-infarct BZ mass cut-off values ranging from 10% to 17% for MCLE and IR-FGRE for 25 study subjects. Due to errors that occurred in creating the heart models, two patients out of 27 were excluded from this analysis.

	MCLE		IR-FGRE	
BZ/LVM (%)	**Sensitivity (%)**	**Specificity (%)**	**Sensitivity (%)**	**Specificity (%)**
10	91.7	25	75	50
11	83.3	33.3	75	58.3
12	75	33.3	66.7	58.3
13	75	58.3	58.3	66.7
14	66.7	75	50	75
15	50	75	41.7	75
16	50	75	41.7	75
17	33.3	83.3	33.3	83.3